Supporting Information

Probing Membrane Receptor - Ligand Specificity with Surface- and Tip-Enhanced Raman Scattering

Lifu Xiao, Karen A Bailey, Hao Wang, Zachary D Schultz*

Department of Chemistry and Biochemistry, University of Notre Dame, Notre Dame, Indiana 46556, USA. E-mail: Schultz.41@nd.edu.

Contents:

Characterization of peptide-functionalized GNPs

The stability of the functionalized GNPs was exhibited by the UV-Vis spectra showing a conserved plasmon resonance peak at around 545 nm (Figure S1a). Average Raman spectra (n=100) of cyclic-RGDFC-GNPs and cyclic-isoDGRFC-GNPs showed a sharp band at 1002 cm^{-1}, corresponding to the characteristic peak of phenylalanine in both ligands, which was not presented in the spectrum of CisoDGRC-GNPs (Figure S1b). The intense broad band at 1550-1600 in all three spectra is assigned to carboxyl group in the peptide ligands [1]. The successful functionalization is also confirmed by dynamic light scattering and zeta potential measurements, showing changes in hydrodynamic diameters and zeta potentials of the functionalized GNPs (Supporting Information, Table S1).

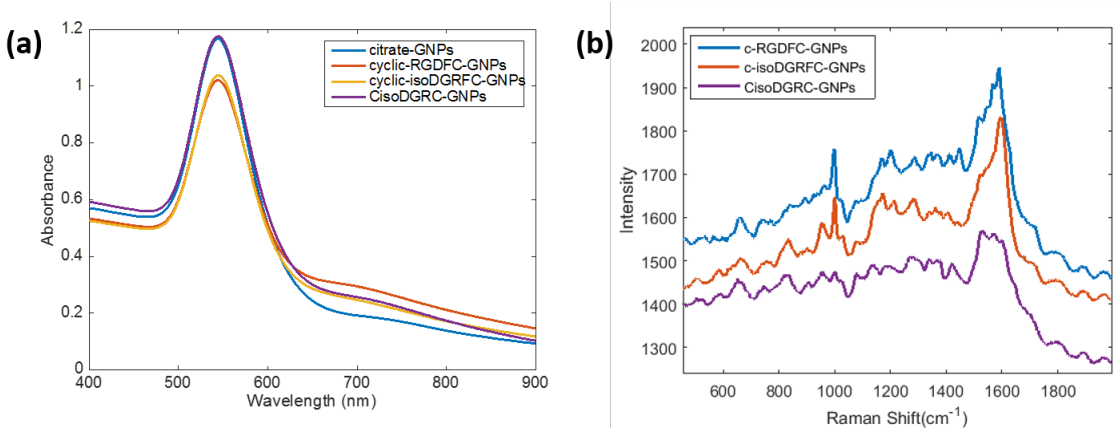

Figure S1. (a) UV-Vis spectra and (b) average Raman spectra of gold nanoparticles with ligands conjugation. The strong Raman band at 1002 cm^{-1} corresponds to the phenylalanine residue present in the ligands.

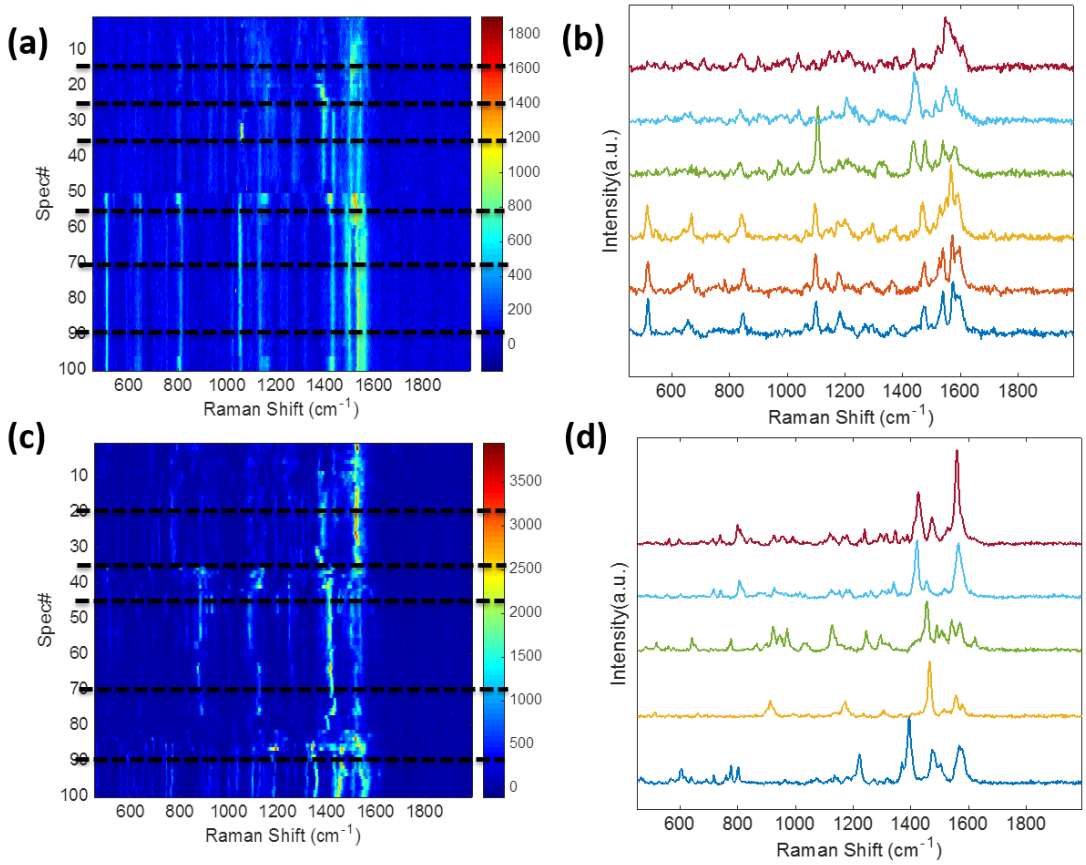

Figure S2. (a, c) Heat maps constructed from 100 consecutive SERS acquisitions of integrin αvβ3-bound cyclic-isoDGRFC-GNPs (a) and CisoDGRC-GNPs (c). (b, d) selected SERS spectra corresponding to dotted lines in (a) and (c).

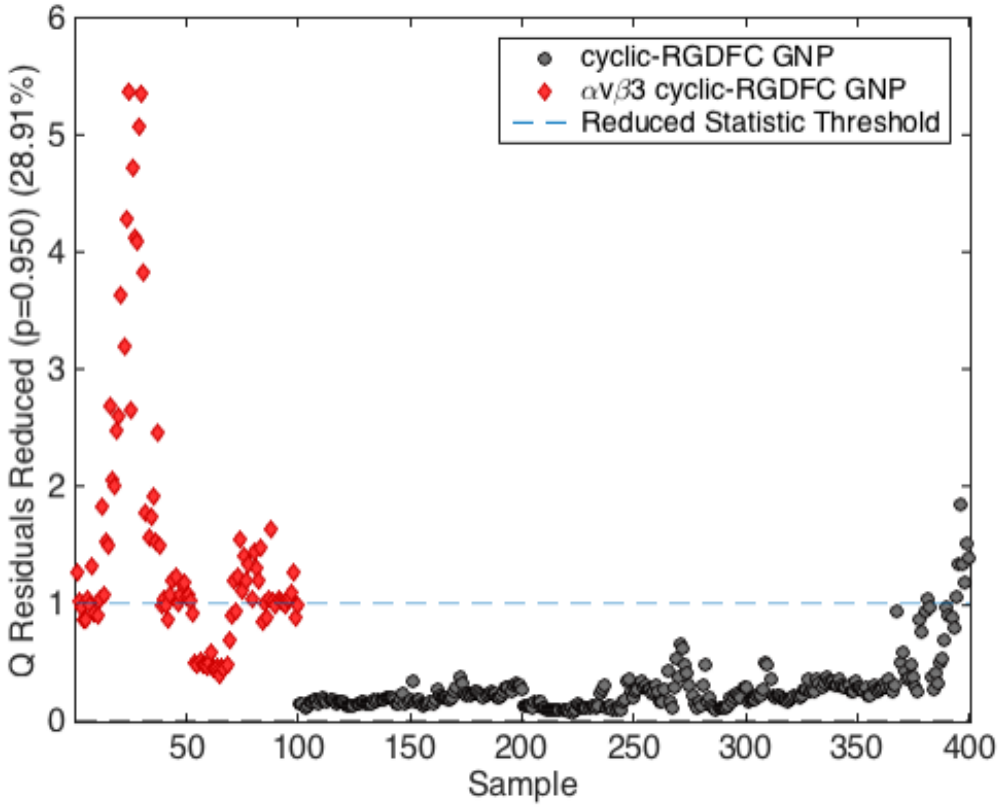

Figure S3. MCR calculated Q residuals from the SERS data shown in Figure 1.

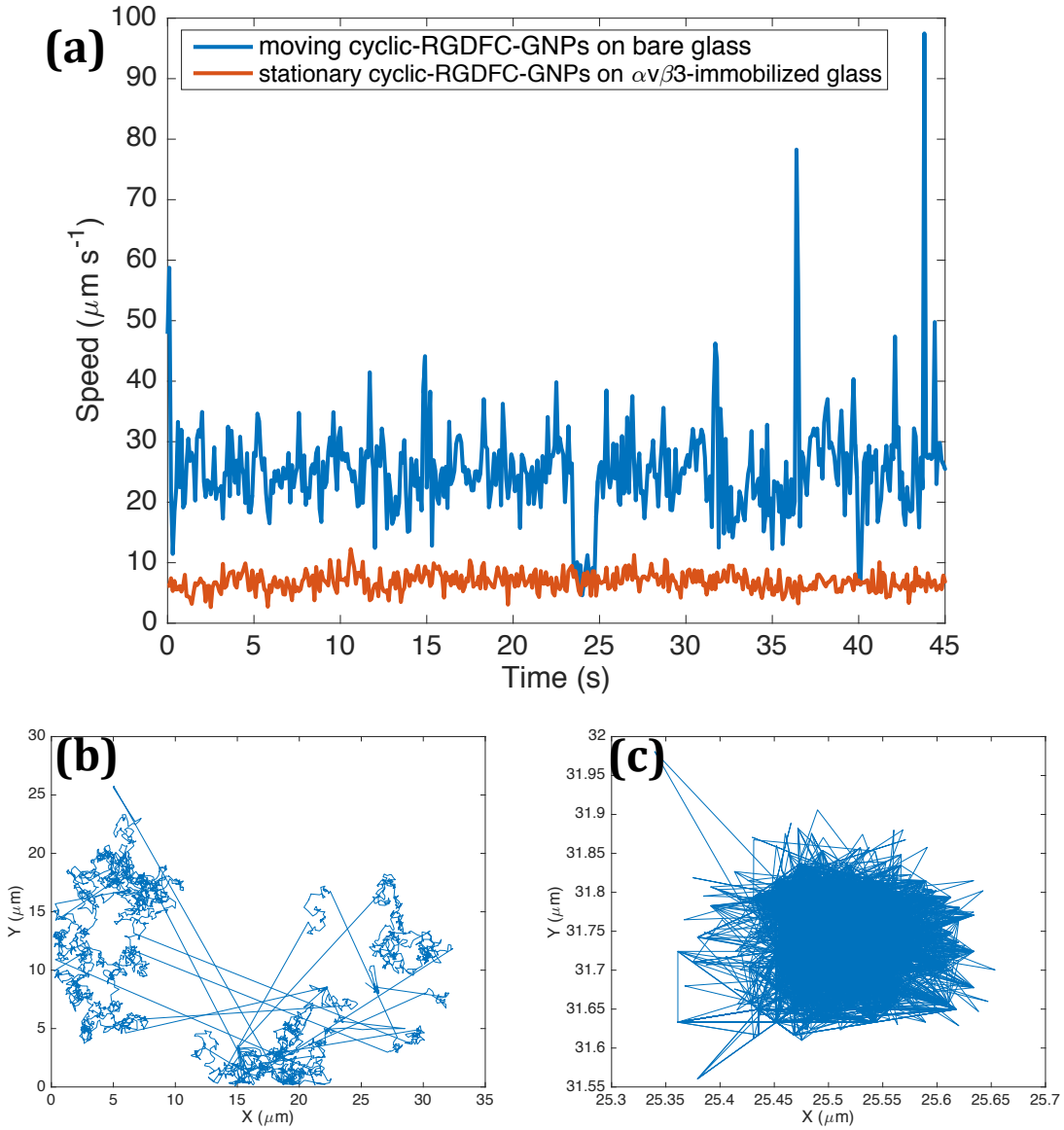

Figure S4. (a) Representative velocity profiles of a cyclic-RGDFC-GNP on bare glass and a stationary GNP on the surface. The velocity of the stationary particle expressed as mean ± standard deviation is 7 ± 1 μm s^{-1}. (b, c) corresponding trajectories of moving (b) and stationary (c) GNPs in (a). The average distances from the centroid of the trajectories for moving and stationary GNPs are 11.51 ± 2.85 μm and 0.06 ± 0.03 μm, respectively.

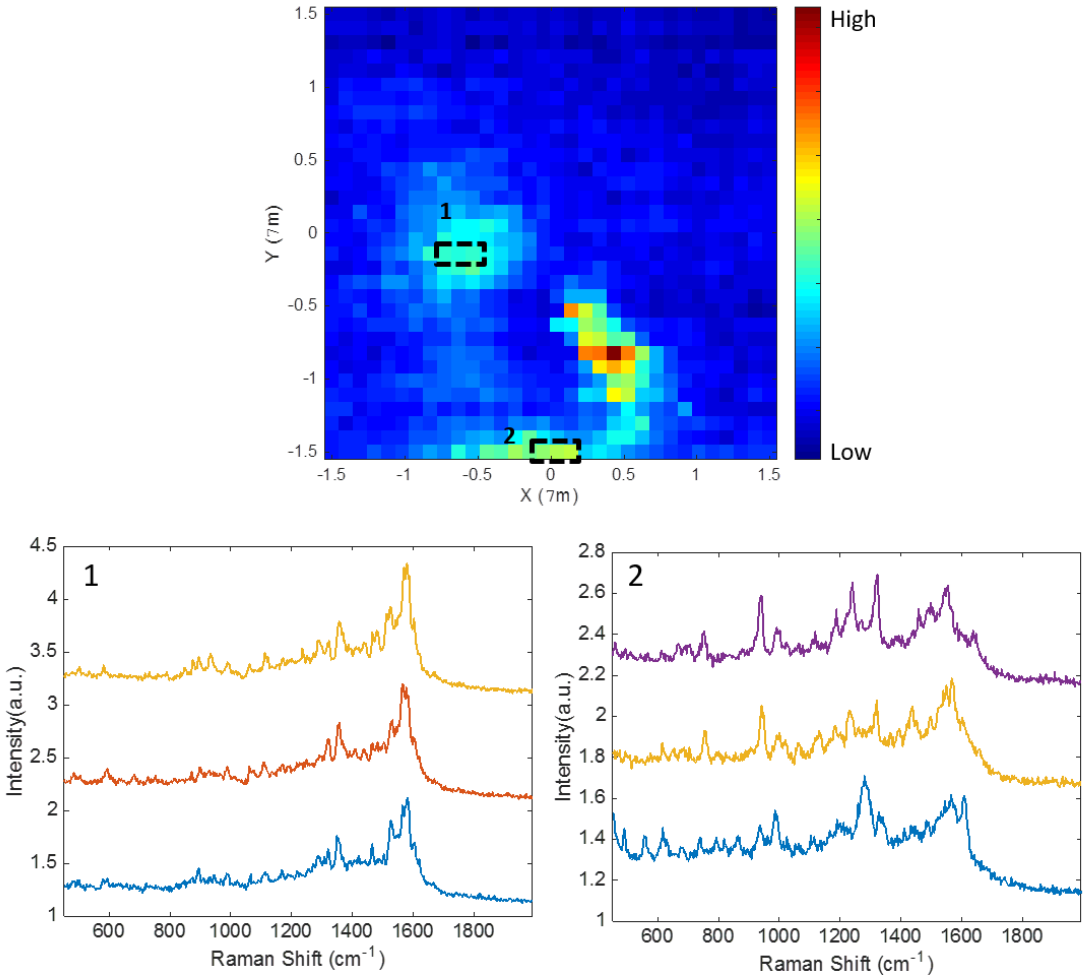

Figure S5. TERS map of cyclic-RGDFC-GNPs bound with sw620 cells. TERS heat map (3x3 μm^2) generated using single-peak intensity at 1002 cm^{-1} and selected TERS spectra corresponding to dashed boxes (1 and 2) in the map.

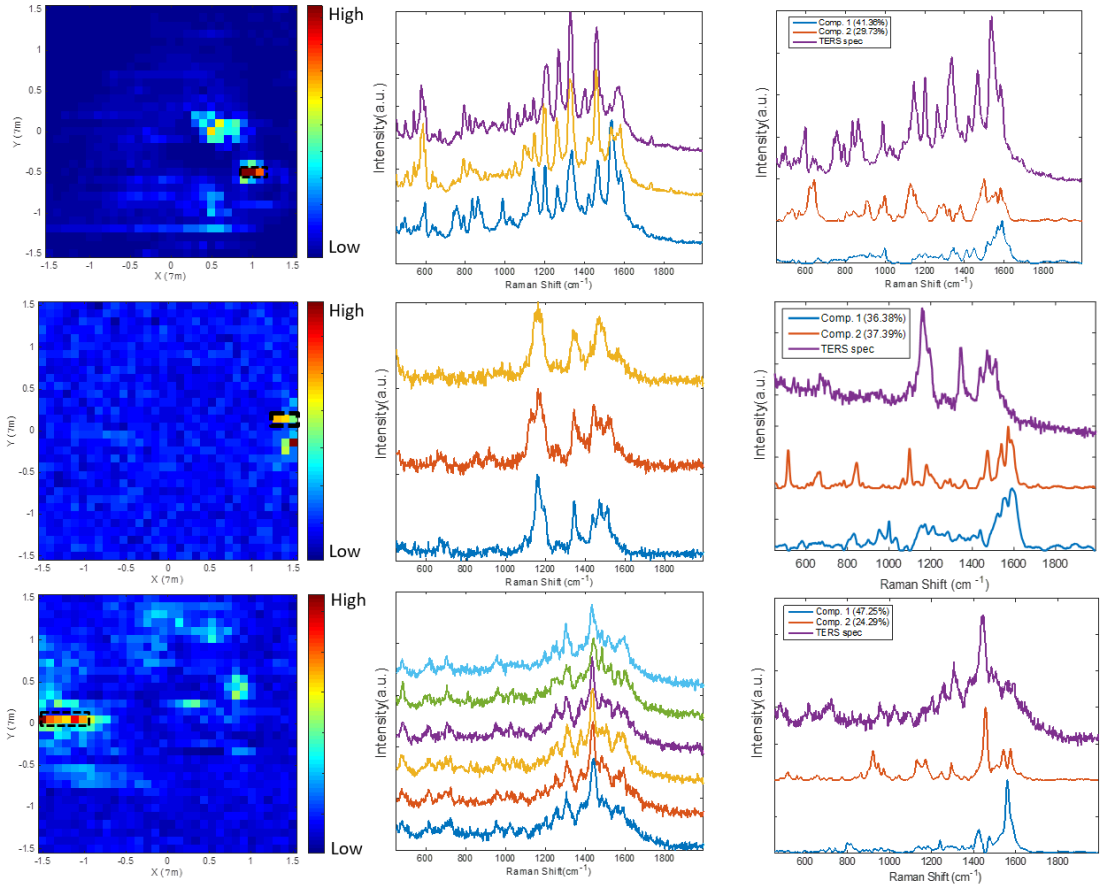

Figure S6. Additional TERS mapping data of SW620 cells incubated with cyclic-RGDFC-GNPs (top), cyclic-isoDGRFC-GNPs (middle) and CisoDGRC-GNPs (bottom). Left: MCR score maps. Middle: TERS spectra. Right: TERS spectrum vs. MCR components.

Hyperspectral imaging

Experiments were performed on an Olympus BX51 microscope. A white light was used for bottom illumination of the SW620 colon cancer cell samples before and after the addition of gold nanoparticles. The scattered light was collected with a water immersion objective (Olympus LUMPLFLN 40XW 0.8 NA), directed into a liquid crystal tunable filter (Channel Systems, VariSpec VIS), and detected by a charge coupled device (CCD) camera (QImaging, Retiga 3000). The filter was tuned from 400 nm to 720 nm at 5 nm intervals with 500 ms acquisition time per frame. Hyperspectral images and scattering spectra were analyzed in ENVI software (Harris Geospatial Solution).

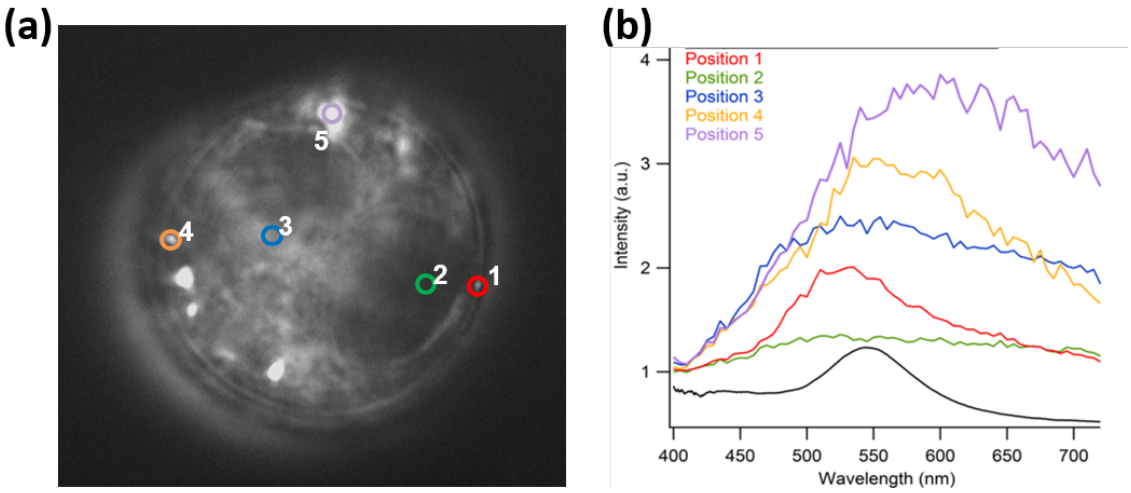

Figure S7. (a) A hyperspectral image with (b) corresponding scattering spectra of a sw620 cell incubated with citrate-GNPs. The black curve in (b) is the spectrum of GNPs.

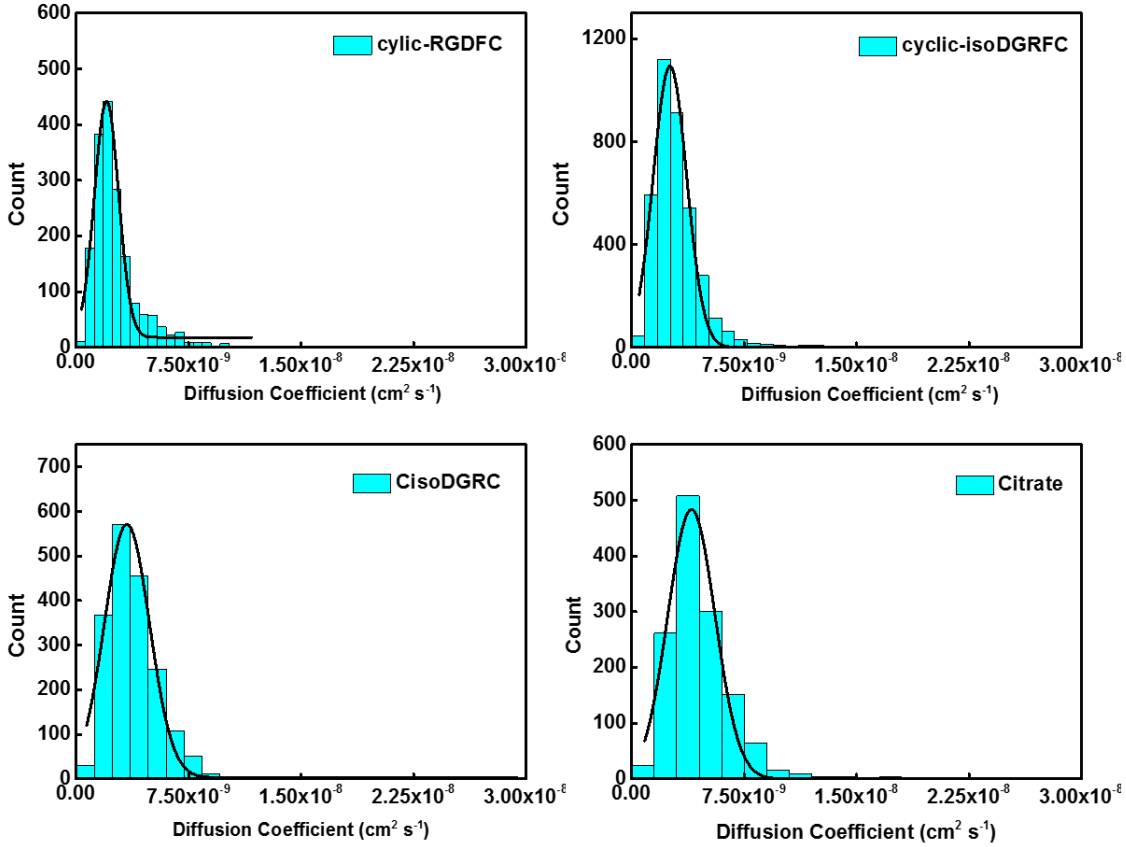

Figure S8. Distribution of diffusion coefficients of ligand-conjugated GNPs interacting with sw620 cells.

Table S1. DLS & zeta potential measurements of gold nanoparticles conjugation with different ligands.

	Size (nm)	**Zeta Potential (mV)**
Citrate-GNPs	91.87 ± 1.11	-58.33 ± 0.76
CisoDGRC-GNPs	89.64 ± 1.08	-53.80 ± 0.62
Cyclic-isoDGRFC-GNPs	87.78 ± 0.52	-49.90 ± 1.56
Cyclic-RGDFC-GNPs	89.00 ± 0.95	-54.83 ± 0.65

Table S2. Raman bands assignments. [1-4]

SERS bands (cm^{-1})	**TERS bands (cm^{-1})**	**Assignments**
515	508	Ser
605-617	588-610, 618	Amide VI
639-641	644	Tyr
844-850	848	Tyr
912	915	Lys
997-1002	990, 1018	Phe, Trp
1067, 1097	1067	Lys
1127	1116	Ser
1152	1149	C-N (Protein)
1170-1176	1176, 1184	Tyr, Phe
1239-1243	1221,	Amide III
1290-1299	1291, 1296	Amide III
1322-1326, 1351-1355	1341, 1367, 1437-1442	CH, CH_2, CH_3
1361-1365	1361	Trp
1456	1465	Lys
1473-1477	1480-1490	Amide II
1499-1502	1514, 1519	C-C, C=C
1542-1544	1542	Amide II
1560, 1572	1562, 1570, 1575	Trp
1579-1582	1595, 1625	Phe, Trp, C-C

REFERENCES

(1) Movasaghi, Z.; Rehman, S.; Rehman, I. U. *Appl. Spectrosc. Rev.* **2007**, *42*, 493-541.

(2) De Gelder, J.; De Gussem, K.; Vandenabeele, P.; Moens, L. *J.Raman Spectrosc.* **2007**, *38*, 1133-1147.

(3) Zhu, G.; Zhu, X.; Fan, Q.; Wan, X. *Spectrochim. Acta, Part A.* **2011**, *78*, 1187-1195.

(4) Deckert-Gaudig, T.; Kurouski, D.; Hedegaard, M. A.; Singh, P.; Lednev, I. K.; Deckert, V. *Sci.Rep.* **2016**, *6*, 33575.